21st IAEA Fusion Energy Conference
Chengdu, China, 16 - 21 October, 2006

IAEA-CN-149/ EX/5-3

# Core Electron-Root Confinement (CERC) in Helical Plasmas

M. Yokoyama et al.

NIFS-837 Oct. 2006

# Core Electron-Root Confinement (CERC) in Helical Plasmas

M. Yokoyama 1), H. Maaβberg 2), K. Ida 1), C.D. Beidler 2), F. Castejon 3), T. Estrada 3), A. Fujisawa 1), T. Minami 1), T. Shimozuma 1), Y. Takeiri 1), V. Tribaldos 3), A.Dinklage 2), S. Murakami 4) and H. Yamada 1)

1) National Institute for Fusion Science, Toki 509-5292, Japan
2) Max-Planck Institut fur Plasmaphysik, Greifswald 17491, Germany
3) Laboratorio Nacional de Fusion, As. EURATOM-CIEMAT, Madrid 28040, Spain
4) Department of Nuclear Engineering, Kyoto Univ., Kyoto 606-8501, Japan

e-mail contact of main author: yokoyama@LHD.nifs.ac.jp

**Abstract.** The improvement of core electron heat confinement has been realized in a wide range of helical devices such as CHS, LHD, TJ-II and W7-AS. Strongly peaked electron temperature profiles and large positive radial electric field, $E_r$, in the core region are common features for this improved confinement. Such observations are consisitent with a transition to the "electron-root" solution of the ambipolarity condition for $E_r$ in the context of the neoclassical transport, which is unique to non-axisymmetric configurations. Based on this background, this improved confinement has been collectively dubbed "core electron-root confinement" (CERC). The electron heat diffusivity is much reduced due to the electron-root $E_r$ compared to that with $E_r$=0 assumed, which clealy demonstrates that 1/ν ripple diffusion (ν being the collision frequency) in low-collisional helical plasmas could be overcome. The magnetic configuration properties play important roles in this transition, and thresholds are found for the collisionality and electron cyclotron heating (ECH) power.

## 1. Introduction

Core electron-root confinement (CERC) is an improved confinement regime which is specific to helical systems. This regime has been obtained in quite different helical devices for ECH discharges above the power threshold depending on the magnetic configuration properties and heating scenarios [1]. It is based on a different mechanism than the internal transport barrier (ITB) in tokamaks, where the strongly sheared $\boldsymbol{E}\times\boldsymbol{B}$ flow within the narrow barrier screens off the turbulent transport; see e.g. the reviews [2,3]. In tokamaks, the ITB physics dominates both the particle and the ion energy balance whereas in helical devices CERC affects primarily the electron energy balance. A comparative study of CERC and ITB features was done for LHD and JT-60U [4].

According to neoclassical (NC) theory for the long-mean-free-path (*lmfp*) regime in helical plasmas, the electron-root $E_r$ is of sufficient magnitude to limit the radial drift of ripple-trapped electrons, and thereby suppresses $1/\nu$ transport [5,6]. Reducing this unfavorable $1/\nu$ transport has been one of the major goals for stellarator optimization [7]. The tailoring of magnetic configurations (quasi-symmetric [8-10] and quasi-isodynamic [11] concepts) has been widely studied to achieve this. The suppression of $1/\nu$ transport via the electron root makes another strategy possible and understanding of CERC physics in the current and future helical devices for such an "electron-root perspective" is one of the main motivations of this international collaboration.

The transitions between "ion-root" (with small magnitude of $E_r$, usually negative) and the "electron-root" (with large $E_r$) are based on a bifurcation mechanism. Such transitions become possible in the NC theory, when the ambipolarity condition of the NC fluxes, in which the transport coefficients depend on $E_r$, allow several (an odd number) solutions. This feature

specific to helical plasmas leads to thresholds with respect to collisionality and ECH power depending on the magnetic configuration and the heating scenarios as well. Close to the thresholds, triggered and spontaneous transitions can be found both in the central potential and in the central $T_e$ profile.

An activity to establish an International Stellarator Profile DataBase (ISPDB) has been initiated. The stellarator-specific CERC physics has been selected as the first topic of this collaboration, for which four helical devices, namely, CHS, LHD, TJ-II and W7-AS, can contribute experimental results.

The documentation and comparison of CERC discharges in these quite different helical devices is the main focus of this paper. In section 2, NC theory in low-collisional helical plasmas is briefly reviewed which is relevant for the CERC interpretation. The characteristics of magnetic configurations in four devices are described in Sec. 3, and CERC features will be documented in Sec.4 with a focus on the effects of the magnetic configuration and heating scenario. Finally, summary and discussion are given in Sec. 5.

## 2. Neoclassical Transport Theory in Low-Collisional Helical Plasmas

Helical devices produce their confining magnetic fields using external coils. Although this has obvious advantages such as steady-state and disruption-free operation, the three-dimensional nature of magnetic fields produces localized particles with large NC transport rates (relative to axisymmetric tokamaks) at fusion-relevant plasma parameters. In the *lmfp* regime in helical plasmas, localized particles experience a uni-directional radial drift until pitch-angle collisions scatter them out of the local magnetic ripple (due to the three-dimensionality of magnetic fields) in which they are trapped. This feature provides the so-called $1/\nu$ regime with less frequent collisions leading to a larger transport. The radial excursion of the localized particles is limited, however, by the presence of $E_r$, as the $\boldsymbol{E}\times\boldsymbol{B}$ drift causes the localized particles to precess poloidally with the frequency $\Omega_E=E_r/rB_0$. For the simplest picture of helical devices, the transport now scales either as $\nu^{1/2}$ or $\nu$, depending on whether collisions or drifts are responsible for removing the particles from local ripples. It is possible to determine the mono-energetic diffusion coefficient, $D$, in each of these three *lmfp* regimes from asymptotic solutions of the kinetic equation and the scalings obtained may be summarized as [5,12]

$$D_{1/\nu} \propto \frac{\kappa^2}{\nu}\varepsilon_{\mathrm{eff}}^{3/2} \qquad D_{\sqrt{\nu}} \propto \frac{\kappa^2\sqrt{\nu}}{\left|\Omega_E\right|^{3/2}} \qquad D_{\nu} \propto \left(\frac{\kappa}{\Omega_E}\right)^2 \nu$$

where $\varepsilon_{\mathrm{eff}}$ is the effective ripple for $1/\nu$ transport and $\kappa$ the kinetic energy. These results, when combined with the ambipolarity constraint on the radial particle fluxes, $\Gamma_e=\Gamma_i$, lead to a non-linear equation which can have multiple solutions for $E_r$ [13]. This is a feature of *lmfp* NC transport theory for helical devices which has no counterpart for axisymmetric tokamaks (where the transport coefficients are independent of $E_r$).

Several features can be pointed out at this point which are of relevance to the CERC discharges. Assuming that electrons are in the $1/\nu$ regime and that $T_e \sim T_i$, the $E_r$ must reduce $\Gamma_i$

to the level of $\Gamma_e$ and the electrons are therefore said to be the rate-controlling species. Often in this case, only a single solution for $E_r$ exists, usually negative, which is refereed to as the *ion root*. To a good approximation $v \propto \kappa^{-3/2}$ so that $1/v$ transport coefficients scale as $T^{7/2}$. Any increase in $T_e$ therefore leads to rapid growth in $\Gamma_e$ (assuming other quantities to be unchanged) which the ions must follow. This process requires a reduction in the magnitude of $E_r$ since even if $T_i$ increases with $T_e$ the transport coefficients in the $\nu^{1/2}$ or $\nu$ regimes scale only as $T^{5/4}$ and $T^{1/2}$, respectively. At some point, however, a second solution for $E_r$ becomes possible (a third one appears simultaneously but is thermodynamically unstable) which is positive and of larger magnitude so as to suppress $1/v$ transport of electrons. This solution is called the *electron root* and the ions are now the rate-controlling species. The strong reduction of both ion and electron transport coefficients leads to predictions of significantly improved NC confinement when the electron root is realized.

To obtain accurate values for transport coefficients in realistic helical devices, one must employ numerical methods which are capable of accounting for arbitrarily complex magnetic fields [14-17]. These numerical methods have been extensively benchmarked within an international collaboration and exhibit excellent agreement in all cases [18].

It should be emphasized that the NC theory used here is based on the assumption of local transport and is therefore incapable of describing effects of islands or stochastic regions on transport. The source-free treatment of the kinetic equation is also a limitation, particularly in the case of strong local heating of trapped electrons by X2-mode of ECH. Even for O1-mode heating of passing electrons, one must expect the high-energy portion of the distribution function to deviate substantially from Maxwellian. For the discharges produced by strong ECH power described in this paper, one must therefore consider the NC values of $\Gamma_e$ to represent a lower limit on the electron particle and heat fluxes.

## 3. Description of the Four Helical Devices: CHS, LHD, TJ-II and W7-AS

Both CHS (8 field periods) and LHD (10 periods) have magnetic configurations of the $l$=2 heliotron type [19]. The magnetic configurations used for CERC experiments are characterized by the position of the major radius, $R_{ax}$, as: for CHS, $0.921<R_{ax}<0.974$ m and for LHD, $3.50<R_{ax}<3.90$ m. The inward shift of $R_{ax}$ leads to a reduction of $\varepsilon_{eff}$, whereas an outward shift results in a strong increase of $\varepsilon_{eff}$ in a large portion of plasma minor radius.

TJ-II is a flexible heliac with 4 field periods where the bean-shaped flux surfaces rotate around the central conductor, composed of a circular and a helical coil. The ratio of the currents in the central conductors allows large variation of the rotational transform, the plasma position, shape, and size to some extent [20]. The rotational transform profile is fairly flat (low shear).

The magnetic configuration of W7-AS is partly drift optimized because of an average elongation of ~2. This averaged elongation reduces both the Shafranov shift and the NC

transport in the Pfirsch-Schlüter as well as in the plateau regime, but not in the *lmfp* regime where localized ripples dominate. With increasing the rotational transform (and outward shift), the localized minima of $B$ deepen, in particular, at outer radii, and dominate the *lmfp* NC transport. In the CERC discharges, mainly low-$\iota$ configurations were employed. In addition to the inward shift, a separated coil current supply allows for an independent variation of the toroidal mirror component controlling the power absorption for trapped electrons for ECH X2-mode. The standard configuration with $\iota(0)/2\pi$~1/3 has a pronounced minimum of $B$ in the ECH launching plane.

The $\varepsilon_{eff}$ in the core region (where CERC is established) in the four devices are summarized here. It is commonly rather low in the CERC region compared to the peripheral region. In LHD, $\varepsilon_{eff}$ takes the smallest value at $R_{ax}$=3.75m (close to zero), and both inward and outward shift of $R_{ax}$ increases $\varepsilon_{eff}$ due to the presence of the toroidal mirror component [21]. TJ-II takes the largest value of $\varepsilon_{eff}$ at the core region (~0.03) among the four devices, and thus, it is expected to have the easiest access to the electron root. In W7-AS, the $\varepsilon_{eff}$ is moderate in the core region [$\varepsilon_{eff}(0)<0.015$] and increases only slowly with radius compared to the other configurations. The low-mirror configuration realized by the corner-coil current control has somewhat smaller $\varepsilon_{eff}$ in the core region.

ECH operation modes and diagnostic equipment relevant to CERC are described in detail in Ref. [1] and they are not repeated here.

## 4. CERC Descriptions

Figure 1 shows examples for $T_e$ profiles in CERC discharges in the four devices. Within the CERC region, $T_e$ is highly peaked. This feature is found at quite different $n_e$, $P_{ECH}$ (ECH power), and $B$, for example, as for the range of $n_e$, $n_e$~$0.15\times10^{19}$m$^{-3}$ (at LHD) to $n_e$~$5.3\times10^{19}$m$^{-3}$ (at W7-AS). With increasing $n_e$ at fixed $P_{ECH}$, however, the $T_e$-profile peaking becomes less pronounced. Figure 2 documents the CERC establishment due to the increase of $P_{ECH}$ at LHD [22] ($n_e$~$0.3\times10^{19}$m$^{-3}$, $B$~1.5T, $R_{ax}$=3.8 m).The power threshold for CERC establishment at these conditions was found to exceed $P_{ECH}$>0.58 MW. The peaked central $T_e$

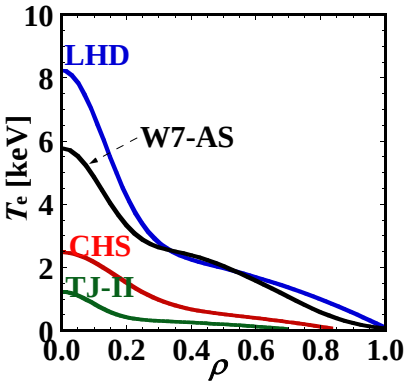


*Fig.1 $T_e$ profiles for example CERC discharges in the four devices.*

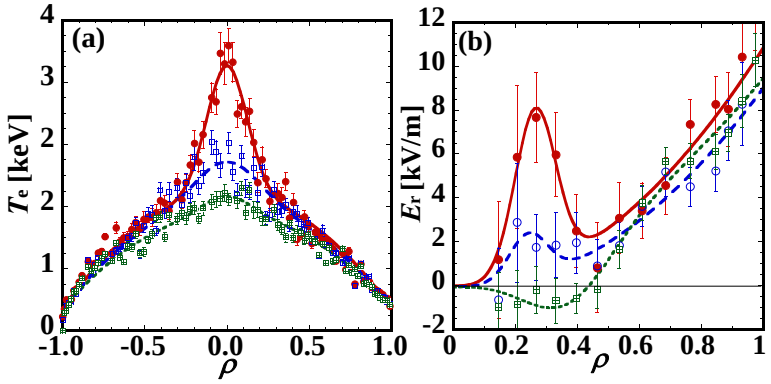


*Fig.2 (a) $T_e$ and (b) $E_r$ profiles measured at LHD with $P_{ECH}$=0, 0.58, and 0.78 MW (from low to high $T_e(0)$) on an NBI sustained plasma.*

profile (Fig. 2(a)) with the additional ECH corresponds to the peak in the electron-root $E_r$ profile (Fig. 2(b)) roughly in the same radial range.

Figure 3 shows results from an ECH power scan experiment at LHD [23] ($R_{ax}$=3.75 m, $B$=1.52 T), where the normalized scale length of the $T_e$ gradient, $R/L_{Te}$ ($R$ is the major radius), is shown as a function of $P_{ECH}/n_e$. It shows a clear jump at the threshold at $P_{ECH}/n_e$~$1.4\times10^{19}$MWm$^3$. This finding indicates that the CERC establishment is based on a bifurcation mechanism. On the contrary, no clear ECH power threshold exists in tokamak electron-ITB formation [4], which reflects that the CERC establishment is based on the stellarator-specific physics, that is, the bifurcation of the NC ambipolar $E_r$ to the electron root. The ECH power threshold is found to increase with $n_e$ [24-26]. Consequently, the $n_e$ threshold for fixed $P_{ECH}$ is also demonstrated at LHD [26], TJ-II [27] and W7-AS [28].

The effect of the magnetic configuration properties, in particular, of $\varepsilon_{eff}$ (in connection to the 1/ν NC diffusion) as well as of the ECH power absorption by ripple-trapped electrons in the CERC region, has been analyzed in LHD and in W7-AS. It is expected that CERC is more easily established in configurations with larger $\varepsilon_{eff}$ due to easier access to the electron-root regime as predicted by NC theory (see Sec. 2) and also as experimentally verified at the peripheral region in LHD [29]. Thus, the threshold with respect to $P_{ECH}$ ($n_e$) should become lower (higher) in configurations with larger $\varepsilon_{eff}$.

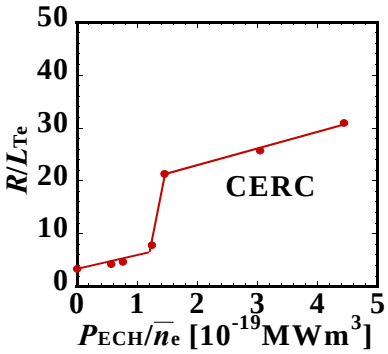


*Fig.3 Normalized $T_e$ gradient as a function of normalized ECH power for X2-mode CERC in LHD ($R_{ax}$=3.75m, B=1.52T)*

This expectation is experimentally verified with the CERC discharges produced by the O1-mode ECH in W7-AS [30], as shown in Fig. 4. The ECH in O1-mode is nearly completely absorbed by passing electrons, and the effect of $\varepsilon_{eff}$ on the CERC establishment could be analyzed. The CERC feature was clearly obtained in a configuration with larger $\varepsilon_{eff}(0)$~0.011 (solid curve in Fig. 4) for the same level of $P_{ECH}$ and $n_e$ compared to the lower $\varepsilon_{eff}(0)$~0.008 configuration (dotted curve in Fig. 4). For the X2-mode ECH, both $P_{ECH}$ and $n_e$ scans were performed [28] for two magnetic configurations: with a minimum of $B$ of ~4.5% ("standard" configuration) and with a maximum of $B$ ("low-mirror" configuration) in the ECH launching plane. Figure 5 shows the results of $P_{ECH}$ scan at fixed $n_e$~$2\times10^{19}$m$^{-3}$. Whereas for the "standard" configuration, the CERC feature appears except for the lowest $P_{ECH}$, it appears only at the highest $P_{ECH}$ in the "low-mirror" configuration. Monte Carlo simulations (by the GNET code [31]) have shown that the ECH-driven electron flux is of

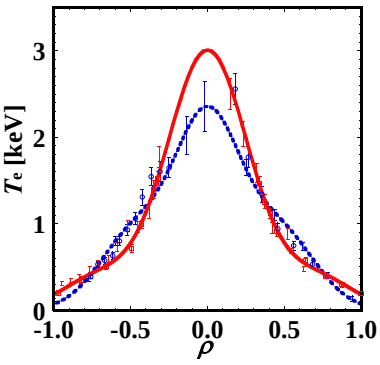


*Fig.4 CERC-$T_e$ profiles obtained in W7-AS (O1-mode ECH). The dotted (solid) curve is for $P_{ECH}$=0.69 (0.65) MW at $n_e(0)$~4 (5)$\times10^{19}$m$^{-3}$ in configurations with $\varepsilon_{eff}(0)$~0.008 (0.011).*

comparable magnitude with the ambipolar NC electron flux in the ion-root region and is also larger in the "standard" configuration than in the "low-mirror" configuration, as confirmed by the faster $T_e$ decay after the switching-off of ECH [28]. Thus the convective electron flux also affects the accessibility to CERC establishment for the X2-mode heating scenario.

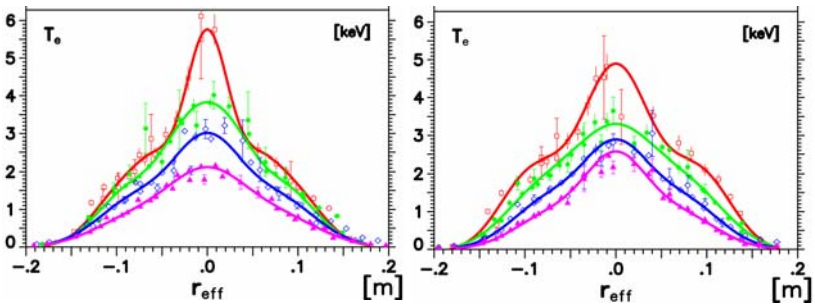


*Fig.5 $T_e$ profiles in ECH power scan experiments ($P_{ECH}$=0.2,0.4, 0.8, and 1.2 MW, from low to high $T_e$) at X2-mode heating in W7-AS for the standard (left) and the low-mirror(right) configurations.*

Large positive $E_r$ (electron root) in the CERC region is commonly observed in four devices. These findings are consistent with the picture of the NC ambipolarity (see. Sec. 2). Figure 6 shows example of the measured $E_r$ values for a CERC discharge in W7-AS in comparison to the NC ambipolar $E_r$ calculated with the measured density and temperature profiles. DKES code results were the basis for the NC particle flux evaluation. Several roots are found from the ambipolarity condition in this local approach, and the transition between the ion root and electron root (solid line) is obtained from the diffusion equation for $E_r$ [32]. The radial bifurcation nature of the ambipolar $E_r$ is confirmed in other devices as well to be the common physical mechanism for the CERC establishment.

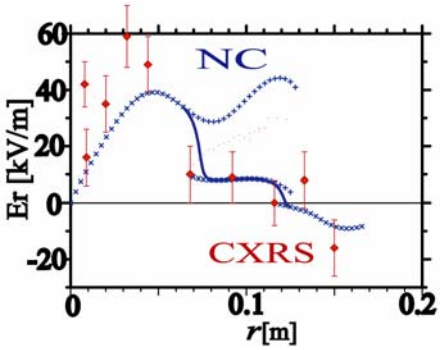


*Fig.6 Measured Er values with the NC ambipolar Er in a CERC discharge in W7-AS.*

The electron energy balance has also been intensively analyzed for CERC discharges and compared with the NC prediction. The traditional picture has been employed here, where a purely diffusive ansatz for the electron heat flux density, $Q_e=-n_e\chi_e T_e'$, is used for the experimental power balance, and $\chi_e(r)$ (the experimental electron heat diffusivity) is compared with the NC heat diffusivity. Figure 7 shows the comparison of the experimental $\chi_e$ (error bars are estimated by least-squares fitting of the power balance) with the NC heat diffusivity in the same discharge as in Fig. 6. The NC $\chi_e$ curve shown for the assumption $E_r$=0 is provided as a theoretical "extension" of the expected electron heat diffusivity under ion root assumptions. The experimental $\chi_e$ is far below this curve, demonstrating that the 1/ν ripple transport can be suppressed with the

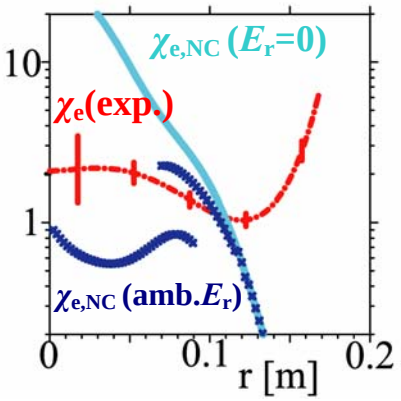


*Fig.7 Comparison between the experimental (exp.) and NC $\chi_e$ with and without considering the ambipolar Er for the same CERC discharge as in Fig.6.*

CERC establishment. The NC bifurcation picture is also confirmed in spontaneous transitions where the central electrostatic potential (measured by Heavy Ion Beam Probe, HIBP) changes in an equivalent manner to the central $T_e$ (measured by Electron Cyclotron Emission) and anti-correlated to the central $n_e$ (proportional to the HIBP intensity) [33].

The impact of magnetic islands on the CERC establishment has also been recognized both at LHD [25,34] and TJ-II [35,36]. The low-order ($\iota/2\pi=1/2$) rational surface is located at the central region in LHD. The NBI-beam driven current can change its location and even make it disappear (in the case of the co-injection) with the modification of rotational transform value/profile. The clear threshold for the ECH power can be observed in the case of the counter-injection. On the other hand, it becomes unclear for the case of co-injection. This difference appear to be related to the presence of the $\iota/2\pi=1/2$ surface in the core region. In TJ-II, high configuration flexibility has been utilized to investigate the impact of low-order rational surfaces. A small inductive current is applied to vary the core rotational transform profile, which demonstrates the reduction of ECH power threshold for the CERC establishment when the $\iota/2\pi=3/2$ island is present in the central part of the discharge [33]. Systematic experiments with different low-order rationals have exhibited a dependence of the threshold density on the order of the rational surface (island width) [36].

## 5. Conclusion and Discussions

Core electron-root confinement (CERC) has been commonly found in the four helical devices, CHS, LHD, TJ-II and W7-AS. CERC is clearly identified as an improved electron energy confinement related to the transition to the electron-root solution of the ambipolarity condition, as predicted by NC transport theory in low-collisional helical plasmas. Configurations with a large effective ripple in the core region allow for easier access to CERC. In particular, TJ-II with the largest $\varepsilon_{eff}(0)$ among the four devices finds CERC at higher collisionality whereas CHS and LHD with lower $\varepsilon_{eff}(0)$ achieve CERC at lower collisionality. For ECH in X2-mode with significant absorption by ripple-trapped electrons, additional ECH-driven flux can reduce the ECH power threshold for CERC establishment, as was found in the W7-AS configuration scan. The impact of rational surfaces on CERC establishment has also been recognized in both LHD and TJ-II experiments.

Some remarks on the CERC accessibility in the future devices are made. For quasi-axisymmetric configurations, like NCSX [9], the ECH power threshold is expected to increase due to its rather low $\varepsilon_{eff}(0)\sim0.002$. On the contrary, quasi-isodynamic configurations allow for a moderate $\varepsilon_{eff}$ at the core region due to the toroidal mirror field. For example, the configurational flexibility of W7-X [7] allows for a variation of the toroidal mirror field, resulting in the variation of $\varepsilon_{eff}(0)$ from 0.0 to 0.025 without affecting a highly peaked ECH deposition. Together with the significant ECH power (up to 10 MW), CERC will probably be possible at higher densities than in the experiments described here.

**References**

[1] YOKOYAMA, M., et al., Fusion Sci. Tech. to appear in **50** (2006) 327.
[2] WOLF, R.C., Plasma Phys. Contr. Fusion **45** (2003) R1.
[3] CONNOR, J.W., et al., Nucl. Fusion **44** (2004) R1.
[4] K. IDA et al., Plasma Phys. Control. Fusion **46**, A45 (2004).
[5] GALEEV, A.A., and SAGDEEV, R.Z., Review of Plasma Physics **7** (1977) 307.
[6] KOVRIZHNYKH, L.M., Nucl. Fusion **24** (1984) 851.
[7] GRIEGER, G., et al., 13th International Conference Plasma Physics Controlled Nuclear Fusion Research, Washington, 1990 (IAEA, Vienna, 1991), Vol.3, p.525.
[8] ALMAGRI, A.F., et al., IEEE Tran. Plasma Sci. **27** (1999) 114.
[9] NEILSON, G.H., et al., Phys. Plasmas **7** (2000) 1911.
[10] SPONG, D.A., et al., Nucl. Fusion **45** (2005) 918.
[11]GORI, S., et al., "Quasi-isodynamic Stellarators," Theory of Fusion Plasmas (Varenna 1996), Editrice Compositori, Bologna (1996), p.335.
[12] BEIDLER, C.D., et al., Plasma Phys. Control. Fusion **36** (1994) 317.
[13] MYNICK, H.E., et al., Nucl. Fusion **23** (1983) 1053.
[14] van RIJ, W.I., et al., Phys. Fluids B **1** (1989) 563.
[15] TRIBALDOS, V., Phys. Plasmas **8** (2001) 1229.
[16] MURAKAMI, S., et al., Nucl. Fusion **42** (2002) L19.
[17] NEMOV, V.V., et al., Phys. Plasmas **6** (1999) 4622.
[18] BEIDLER, C.D., et al., 30th EPS Conf. Plasma Phys. Contr. Fus., St Petersburg 2003, http://epsppd.epfl.ch/StPetersburg/pdf/P3_002.pdf.
[19] UO, K., J. Phys. Soc. Japan **16** (1961) 1380.
[20] TRIBALDOS, V., et al., Nucl. Fusion **36** (1996) 283.
[21] YOKOYAMA, M., et al., Nucl. Fusion **45** (2005) 1600.
[22] IDA, K., et al., Phys. Rev. Lett. ***91*** (2003) 085003.
[23] IDA, K., et al., Phys. Plasmas **11** (2004) 2551.
[24] TAKEIRI, Y., et al., Phys. Plasmas **10** (2003) 1788.
[25] TAKEIRI, Y., et al., Fusion Sci. Techn. **46** (2004) 106.
[26] SHIMOZUMA, T., et al., Plasma Phys. Control. Fusion **45** (2003) 1183.
[27] CASTEJON, F., et al., Nucl. Fusion **42** (2002) 271.
[28] MAAβBERG, H., et al., Phys. Plasmas 7 (2000) 295.
[29] YOKOYAMA, M., et al., J. Plasma Fusion Res. SERIES **6** (2004) 218.
[30] ROMÉ, M., et al., Plasma Phys. Control. Fusion **48** (2006) 353.
[31] MURAKAMI, S., et al., Nucl. Fusion **40** (2000) 693.
[32] MAAβBERG, H., et al., Phys. Fluids B **5** (1993) 3627.
[33] ESTRADA, T., et al., Plasma Phys. Control. Fusion **46** (2004) 277.
[34] SHIMOZUMA, T., et al., Nucl. Fusion **45** (2005) 1396.
[35] CASTEJON, F., et al., Nucl. Fusion **44** (2004) 593.
[36] ESTRADA, T., et al., Fusion Sci. Tech. **50** (2006) 127.